Short-wave instability due to wall slip and numerical observation of wall-slip instability for microchannel flows

By CAI-JUN GAN AND ZI-NIU WU†

Department of Engineering Mechanics, Tsinghua University, Beijing 100084, PR China

The stability of an incompressible parallel flow with a linear wall slip – where the amount of wall slip is proportional to the velocity gradient – is analysed. Numerical computations are performed for microchannel flows in the slip-flow region. The wall slip causes short-wave instability while the slip-flow model is stable for long waves. This instability disappears once the slip wall condition is replaced by the no-slip condition.

1. Introduction

There are several important applications in which there is a tangential slip on the wall for the velocity of a viscous fluid. The first example is polymer melts which exhibit wall slip (see for instance Morton 2001). The second example is some biological and even technological drag reduction surfaces in which there is a slip (see for instance Hoyt 1975; Bechert *et al.* 2000). The third example is high-speed rarefied flow for which rarefaction leads to wall slip (Kennard 1938; Bird 1994), as in the case of hypersonic re-entry flow at an altitude of 30 km–60 km. The example with which we are concerned here is the microchannel flow for a Knudsen number larger than a critical value.

The relation between the amount of wall slip and the gradient of the tangential velocity is of special importance. For rarefaction-induced slip, such as microflows and for high-speed rarefied flows, within a first order of approximation, the amount of slip is linearly proportional to the gradient of the tangential velocity at the wall, with the proportionality coefficient defined as the slip length (Kennard 1938; Karniadakis & Beskok 2002). The slip length is proportional to the Knudsen number (Kn), which is defined as the ratio between the mean-free path of gas molecules and the characteristic length scale of the flow. Molecules impinging on a solid wall lose only a part of their tangential momentum, which macroscopically manifests as a velocity slip. Microflows have important applications in microelectromechanical (MEMs) systems and the study of microflows has become an active area of research, revealing many new behaviours such as lower speed rarefaction, lower speed compressibility, viscous heating and thermal creep for gas micro flows, wetting, adsorption and electrokinetics for liquid micro flows. For details of this topic see, for instance, Bird (1994), Ho & Tai (1998), Gad-el-Hak (1999), Cercignani (2000), and Karniadakis & Beskok (2002).

In this paper, we are interested in the problem of stability due to a linear wall slip, that is, the amount of slip is linearly proportional to the gradient of the tangent

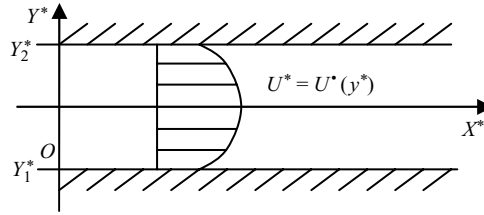† Author to whom correspondence should be addressed: ziniuwu@tsinghua.edu.cn.

FIGURE 1. Flow in a channel.

velocity. This is important in microflows which display linear velocity slip on the wall for moderate Knudsen numbers.

The model suitable for describing microflows is different from that for macroflows. The choice of the model depends on the Knudsen number (Kn). The Navier–Stokes equations are valid for $Kn < 0.01$ if no-slip wall conditions are used, and the validity regime extends to $0.01 < Kn < 0.1$ if slip wall conditions are used (see, for instance, Karniadakis & Beskok 2002). For Kn higher than 0.1 (sometimes slightly different values are used), the flow is in the so-called transition regime and more complex models such as the Boltzmann equation or Burnett equations, super-Burnett equations, and so on, should be used (Cercignani 2000).

In order to analyse the instability due to wall slip theoretically, we will consider an incompressible parallel-flow model. The incompressible slip-flow model can be considered as a limiting case of the compressible slip-flow model with a vanishing Mach number. Both long-wave and short-wave stability analyses will be performed. The Orr–Sommerfeld equation for stability analysis is the same as for classical instability analysis. The only new feature is that a slip condition is associated with the boundary. The techniques used here are standard, and can be found in Lin (1955), Betchov & Criminale (1967), Drazin & Reid (1981), Shivamoggi (1986), and Schmid & Henningson (2001). For long-wave stability analysis, we will consider a general velocity profile, while for short-wave stability analysis we consider a specific velocity profile. Since Poiseuille flow is typical of microchannel flow, we will simply consider a Poiseuille profile (with correction due to wall slip) for short-wave stability analysis. Details of the analysis will be presented in §2.

In §3, we perform numerical experiments for flows with a velocity slip. The numerical experiments will be based on a carefully chosen scheme for which we shall test that the instability is not due to pure numerical treatment. We will verify that the instability is due to wall slip and that it is a short-wave instability, as predicted theoretically. Concluding remarks will be provided in §4.

2. Stability analysis for an incompressible slip-flow model

2.1. *The incompressible slip-flow model*

Consider a channel as shown in figure 1. The velocity vector of the basic flow is given by $(U^*, 0, 0)$ where $U^* = U^*(y^*)$. The incompressible Navier–Stokes equations used for stability analysis here are given by

$$\frac{\partial u_k^*}{\partial x_k^*} = 0, \tag{1}$$

$$\rho^* \frac{\partial u_i^*}{\partial t^*} + \rho^* u_k^* \frac{\partial u_i^*}{\partial x_k^*} = -\frac{\partial p^*}{\partial x_i^*} + \frac{\partial}{\partial x_k^*}\left[\mu\left(\frac{\partial u_i^*}{\partial x_k^*} + \frac{\partial u_k^*}{\partial x_i^*}\right)\right], \tag{2}$$

where ρ^* is the density, p^* is the dynamic pressure, μ is the dynamic viscosity coefficient and u_i^* is the velocity component in the direction x_i^*. Alternatively, we also use (u^*, v^*, w^*) to denote (u_1^*, u_2^*, u_3^*), and (x^*, y^*, z^*) to denote (x_1^*, x_2^*, x_3^*).

The linear slip boundary condition used for stability analysis is given by

$$u^* = b^* \frac{\partial u^*}{\partial y^*}, \quad \text{on the wall} \tag{3}$$

where b^* is the slip length.

For non-dimensional treatment, we use the following parameters,
   (i) velocity $U_0 = \max_{y_1^* < y^* < y_2^*}(U^*(y^*))$;
  (ii) length (half-channel height) $H = (y_2^* - y_1^*)/2$;
 (iii) time $T = H/U_0$;
 (iv) pressure $P_0 = \rho^* U_0^2$.
The non-dimensional values are defined by

$$u_i = u_i^*/U_0, \quad x_i = x_i^*/H, \quad t = t^*/T, \quad p = p^*/P_0.$$

The non-dimensional form of (3) can be written as

$$u = b \frac{\partial u}{\partial y}, \quad \text{on the wall}, \tag{4}$$

and $b = b^*/H$. If $b = 0$, (4) is the so-called no-slip wall condition.

The normal velocity must vanish,

$$v = 0 \text{ on the wall}. \tag{5}$$

2.2. *The Orr–Sommerfeld equation and its boundary condition*

We adopt the method based on linear normal modes analysis to study instability. For limitations of linear hydrodynamic stability analysis, see Grossmann (2000).

If α denotes the wavenumber, and c denotes the wave speed, the Orr–Sommerfeld equation used to study stability can be written as

$$(D^2 - \alpha^2)^2 \phi = iRe\,\alpha[(U - c)(D^2 - \alpha^2) - D^2 U]\phi. \tag{6}$$

Here, $Re = \rho^* H U_0/\mu$ is the Reynolds number, the operator D is defined as $D = d/dy$.

It should be noted that the Orr–Sommerfeld equation does not contain the slip length explicitly. The slip length is involved both through the velocity profile and through the boundary condition which, by using (4) and (5), can be written as

$$\phi = 0, \quad y = \pm 1, \tag{7}$$
$$D\phi = \mp b D^2 \phi, \quad y = \pm 1. \tag{8}$$

We must pay attention to the sign of the right-hand side of (8) for the upper wall ($y = +1$).

2.3. *Short-wave instability for Poiseuille flow*

The velocity profile for an incompressible Poiseuille flow including the effect of velocity slip (4) can be obtained easily as

$$U = \frac{1 + 2b - y^2}{1 + 2b}, \quad -1 \leqslant y \leqslant 1. \tag{9}$$

See Arkilic, Schmidt & Breuer (1997) for more details on the derivation of the velocity distribution functions in a microchannel.

We consider the limiting case of short-wave instability, for which $\alpha \to \infty$. In order to study the short-wave instability, we expand the modes in terms of a small parameter $(i\alpha)^{-1}$. This can be similarly done as instability analysis for large-Reynolds-number flow, where the modes are expanded in terms of $(i\alpha Re)^{-1/2}$. The subsequent analysis holds only when the slip length b is large enough so that the condition

$$b\alpha \gg 1 \tag{10}$$

holds. Hence, the present analysis does not hold for the case $b = 0$.

2.3.1. *Solution of the Orr–Sommerfeld equation for short-wave modes*

Following Heisenberg (1924), let

$$\phi = \exp\left(\int g(y)\,dy\right), \tag{11}$$

where $g(y)$ is also a function of α and satisfies the third-order nonlinear equation

$$g^4 + 6g^2 g' + 4gg'' + 3g'^2 + g''' - 2\alpha^2(g^2 + g') + \alpha^4$$
$$= i\alpha Re\{(U - c)(g^2 + g' - \alpha^2) - U''\}, \tag{12}$$

where $g' = dg(y)/dy$, $g'' = d^2g(y)/dy^2$, $g''' = d^3g(y)/dy^3$.

Approximation to the solutions of this equation can then be obtained by assuming an expansion of the form

$$g(y) = (i\alpha)g_0 + g_1 + (i\alpha)^{-1}g_2 + (i\alpha)^{-2}g_3 + \cdots. \tag{13}$$

The recognition that the viscous term does not have a corresponding equilibrium term in equation (12) and the wave speed c is a function of α, Kn and Re, yields the following expansion

$$Re\,c = (i\alpha)c_0 + c_1 + (i\alpha)^{-1}c_2 + (i\alpha)^{-2}c_3 + \cdots. \tag{14}$$

From (14) and $c = c_r + ic_i$, the leading approximations of c_r and c_i can be written as

$$(c_r)_0 = c_1/Re,$$
$$(c_i)_0 = \alpha c_0/Re.$$

Hence, under the limiting case of short-wave $\alpha \to \infty$, if $c_0 > 0$, then $c_i > 0$ and the slip-flow model is unstable; if $c_0 < 0$, then $c_i < 0$ and the slip-flow model is stable.

Inserting (13) and (14) into (12) and comparing the corresponding powers of $(i\alpha)^n$ ($n = 4, 3, 2, 1, \cdots$), we obtain a sequence of equations from which all of the coefficients $g_m(y)$ ($m = 0, 1, 2, 3, \cdots$) can be determined algebraically. In an approximation of this type, only c_0, c_1 are required, and they satisfy the equations

$$(g_0^2 + 1)(g_0^2 + 1 + c_0) = 0, \tag{15}$$
$$4g_0^3 g_1 + 6g_0^2 g_0' + 4g_0 g_1 = (ReU - c_1)(g_0^2 + 1) - c_0(2g_0 g_1 + g_0'), \tag{16}$$

$$\{2g_0^2(2g_0 g_2 + g_1^2) + 4g_0^2 g_1^2\} + 6\{g_0^2 g_1' + 2g_0 g_1 g_0'\}$$
$$+ 4g_0 g_0'' + 3g_0'^2 + 2\{(2g_0 g_2 + g_1^2) + 2g_1'\}$$
$$= (ReU - c_1)(2g_0 g_1 + g_0') - c_0\{(2g_0 g_2 + g_1^2) + g_1'\} - c_2(g_0^2 + 1), \tag{17}$$

$$\{4g_0^2(g_0g_3 + g_1g_2) + 4g_0g_1(2g_0g_2 + g_1^2)\} + 6\{g_0^2g_2 + 2g_0g_1g_1' + (2g_0g_2 + g_1^2)g_0'\}$$
$$+ 4(g_0g_1'' + g_1g_0'') + 6g_0'g_1' + g_0''' + 2\{2(g_0g_3 + g_1g_2) + g_2'\}$$
$$= (ReU - c_1)(2g_0g_2 + g_1^2 + g_1') - c_0(2g_0g_3 + 2g_1g_2 + g_2')$$
$$- c_2(2g_0g_1 + g_0') - c_3(g_0^2 + 1) - ReU''. \tag{18}$$

From equation (15), we see that either $g_0^2 + 1 = 0$ or $g_0^2 + 1 + c_0 = 0$. Obviously, from equation (18), we can have $c_0 \neq 0$. Hence, if $g_0^2 + 1 = 0$, according to (16), (17) and (18), then

$$g_0 = \pm i, \quad g_1 = g_2 = 0, \quad g_3 = \pm i\frac{ReU''}{2c_0}.$$

Setting $c_0 = q^2 - 1$, where q is not equal to 1, the model is unstable if $q > 1$ and stable if $q < 1$. If $g_0^2 + 1 + c_0 = 0$, then by (16), (17) and (18), we have

$$g_0 = \pm qi, \quad g_1 = \mp i\frac{ReU - c_1}{2q}, \quad g_2 = \mp i\frac{(ReU - c_1)^2}{8q^3}(1 - 4q^2c_2),$$

$$g_3 = \pm i\frac{\varsigma\{(1 - 4q^2c_2)(q^2 - 1) - 4q^2 + 8q^4c_2\} + (ReU - c_1)c_2 - (1 - q^2)c_3 - ReU''}{2q(1 - q^2)},$$

$$\varsigma = \frac{(ReU - c_1)^3}{8q^4}.$$

On substituting these results into (13), we obtain the following approximations,

$$g^{1,2} = \mp\alpha \mp i\frac{1}{\alpha^2}\frac{ReU''}{2(q^2 - 1)} + o\left(\frac{1}{\alpha^2}\right), \tag{19}$$

$$g^{3,4} = \mp\alpha q \mp i\frac{ReU - c_1}{2q} + O\left(\frac{1}{\alpha}\right). \tag{20}$$

The above four asymptotic solutions (19) and (20) of the equation $g(y)$ are uniformly valid in the whole domains of the complex plane.

Inserting (19) and (20) into (11) leads to

$$\phi = a_1 \exp(-\alpha y)\exp\left(-i\frac{1}{\alpha^2}\frac{ReU''}{2(q^2 - 1)}y\right)$$
$$+ a_2 \exp(-\alpha qy)\exp\left(-i\frac{Re}{2q}\left\{\frac{k_0}{2}[y^3/3 - (2b+1)y] - \frac{c_1}{Re}y\right\}\right)$$
$$+ a_3 \exp(\alpha y)\exp\left(i\frac{1}{\alpha^2}\frac{ReU''}{2(q^2 - 1)}y\right)$$
$$+ a_4 \exp(\alpha qy)\exp\left(i\frac{Re}{2q}\left\{\frac{k_0}{2}[y^3/3 - (2b+1)y] - \frac{c_1}{Re}y\right\}\right),$$

where $k_0 = -2/(1 + 2b)$.

If we decompose $\phi = \phi_r + i\phi_i$, where ϕ_r and ϕ_i are the real and imaginary parts of ϕ, respectively, we have

$$\phi_r = a_1 e^{-\alpha y}\cos\left(\frac{1}{\alpha^2}\frac{ReU''}{2(q^2 - 1)}y\right) + a_2 e^{-\alpha qy}\cos\left(\frac{Re}{2q}\left\{\frac{k_0}{2}[y^3/3 - (2b+1)y] - \frac{c_1}{Re}y\right\}\right)$$
$$+ a_3 e^{\alpha y}\cos\left(\frac{1}{\alpha^2}\frac{ReU''}{2(q^2 - 1)}y\right) + a_4 e^{\alpha qy}\cos\left(\frac{Re}{2q}\left\{\frac{k_0}{2}[y^3/3 - (2b+1)y] - \frac{c_1}{Re}y\right\}\right), \tag{21}$$

$$\phi_i = -a_1 e^{-\alpha y} \sin\left(\frac{1}{\alpha^2} \frac{ReU''}{2(q^2-1)} y\right) - a_2 e^{-\alpha q y} \sin\left(\frac{Re}{2q}\left\{\frac{k_0}{2}[y^3/3 - (2b+1)y] - \frac{c_1}{Re} y\right\}\right)$$
$$+ a_3 e^{\alpha y} \sin\left(\frac{1}{\alpha^2} \frac{ReU''}{2(q^2-1)} y\right) + a_4 e^{\alpha q y} \sin\left(\frac{Re}{2q}\left\{\frac{k_0}{2}[y^3/3 - (2b+1)y] - \frac{c_1}{Re} y\right\}\right).$$
(22)

2.3.2. Dispersion relation

Substituting (21) into the boundary conditions (7)–(8) yields

$$\left.\begin{array}{l} a_1 e^{-\alpha} \cos\theta_1 + a_2 e^{-\alpha q} \cos\theta_3 + a_3 e^{\alpha} \cos\theta_1 + a_4 e^{\alpha q} \cos\theta_3 = 0, \\ a_1 e^{\alpha} \cos\theta_2 + a_2 e^{\alpha q} \cos\theta_4 + a_3 e^{-\alpha} \cos\theta_2 + a_4 e^{-\alpha q} \cos\theta_4 = 0, \\ a_1 e^{-\alpha} K_{31} + a_2 e^{-\alpha q} K_{32} + a_3 e^{\alpha} K_{33} + a_4 e^{\alpha q} K_{34} = 0, \\ a_1 e^{\alpha} K_{41} + a_2 e^{\alpha q} K_{42} + a_3 e^{-\alpha} K_{43} + a_4 e^{-\alpha q} K_{44} = 0, \end{array}\right\}$$
(23)

where

$$\theta_1 = \frac{Rek_0}{2(q^2-1)\alpha^2}, \quad \theta_1' = \frac{Rek_0}{2(q^2-1)\alpha^2}, \quad \theta_1'' = 0,$$
$$\theta_2 = -\theta_1, \quad \theta_2' = \theta_1', \quad \theta_2'' = 0,$$
$$\theta_3 = -\frac{Re}{2q}\left\{\frac{k_0}{2}(2b+2/3) + (c_r)_0\right\}, \quad \theta_3' = -\frac{Re}{2q}(bk_0 + (c_r)_0), \quad \theta_3'' = \frac{Re}{2q}k_0,$$
$$\theta_4 = \frac{Re}{2q}\left\{\frac{k_0}{2}(2b+2/3) + (c_r)_0\right\}, \quad \theta_4' = -\frac{Re}{2q}(bk_0 + (c_r)_0) \quad \theta_4'' = -\frac{Re}{2q}k_0,$$
$$c_1 = Re(c_r)_0,$$

and

$$K_{31} = -\alpha\cos\theta_1 - \theta_1'\sin\theta_1 + b\{(\alpha^2 - \theta_1'^2)\cos\theta_1 + (2\alpha\theta_1' - \theta_1'')\sin\theta_1\},$$
$$K_{32} = -\alpha q\cos\theta_3 - \theta_3'\sin\theta_3 + b\{(\alpha^2 q^2 - \theta_3'^2)\cos\theta_3 + (2\alpha q\theta_3' - \theta_3'')\sin\theta_3\},$$
$$K_{33} = \alpha\cos\theta_1 - \theta_1'\sin\theta_1 + b\{(\alpha^2 - \theta_1'^2)\cos\theta_1 - (2\alpha\theta_1' + \theta_1'')\sin\theta_1\},$$
$$K_{34} = \alpha q\cos\theta_3 - \theta_3'\sin\theta_3 + b\{(\alpha^2 q^2 - \theta_3'^2)\cos\theta_3 - (2\alpha q\theta_3' + \theta_3'')\sin\theta_3\},$$
$$K_{41} = -\alpha\cos\theta_2 - \theta_2'\sin\theta_2 - b\{(\alpha^2 - \theta_2'^2)\cos\theta_2 + (2\alpha\theta_2' - \theta_2'')\sin\theta_2\},$$
$$K_{42} = -\alpha q\cos\theta_4 - \theta_4'\sin\theta_4 - b\{(\alpha^2 q^2 - \theta_4'^2)\cos\theta_4 + (2\alpha q\theta_4' - \theta_4'')\sin\theta_4\},$$
$$K_{43} = \alpha\cos\theta_2 - \theta_2'\sin\theta_2 - b\{(\alpha^2 - \theta_2'^2)\cos\theta_2 - (2\alpha\theta_2' + \theta_2'')\sin\theta_2\},$$
$$K_{44} = \alpha q\cos\theta_4 - \theta_4'\sin\theta_4 - b\{(\alpha^2 q^2 - \theta_4'^2)\cos\theta_4 - (2\alpha q\theta_4' + \theta_4'')\sin\theta_4\}.$$

Substituting (22) into the boundary conditions (7)–(8) yields

$$\left.\begin{array}{l} -a_1 e^{-\alpha} \sin\theta_1 - a_2 e^{-\alpha q} \sin\theta_3 + a_3 e^{\alpha} \sin\theta_1 + a_4 e^{\alpha q} \sin\theta_3 = 0, \\ -a_1 e^{\alpha} \sin\theta_2 - a_2 e^{\alpha q} \sin\theta_4 + a_3 e^{-\alpha} \sin\theta_2 + a_4 e^{-\alpha q} \sin\theta_4 = 0, \\ a_1 e^{-\alpha} G_{31} + a_2 e^{-\alpha q} G_{32} - a_3 e^{\alpha} G_{33} - a_4 e^{\alpha q} G_{34} = 0, \\ a_1 e^{\alpha} G_{41} + a_2 e^{\alpha q} G_{42} - a_3 e^{-\alpha} G_{43} - a_4 e^{-\alpha q} G_{44} = 0. \end{array}\right\}$$
(24)

Here,

$$G_{31} = \alpha\sin\theta_1 - \theta_1'\cos\theta_1 + b\{(\theta_1'^2 - \alpha^2)\sin\theta_1 + (2\alpha\theta_1' - \theta_1'')\cos\theta_1\},$$
$$G_{32} = \alpha q\sin\theta_3 - \theta_3'\cos\theta_3 + b\{(\theta_3'^2 - \alpha^2 q^2)\sin\theta_3 + (2\alpha q\theta_3' - \theta_3'')\cos\theta_3\},$$
$$G_{33} = \alpha\sin\theta_1 + \theta_1'\cos\theta_1 + b\{(\alpha^2 - \theta_1'^2)\sin\theta_1 + (2\alpha\theta_1' + \theta_1'')\cos\theta_1\},$$
$$G_{34} = \alpha q\sin\theta_3 + \theta_3'\cos\theta_3 + b\{(\alpha^2 q^2 - \theta_3'^2)\sin\theta_3 + (2\alpha q\theta_3' + \theta_3'')\cos\theta_3\},$$

$$G_{41} = \alpha \sin \theta_2 - \theta_2' \cos \theta_2 - b\{(\theta_2'^2 - \alpha^2) \sin \theta_2 + (2\alpha\theta_2' - \theta_2'') \cos \theta_2\},$$

$$G_{42} = \alpha q \sin \theta_4 - \theta_4' \cos \theta_4 - b\{(\theta_4'^2 - \alpha^2 q^2) \sin \theta_4 + (2\alpha q\theta_4' - \theta_4'') \cos \theta_4\},$$

$$G_{43} = \alpha \sin \theta_2 + \theta_2' \cos \theta_2 - b\{(\alpha^2 - \theta_2'^2) \sin \theta_2 + (2\alpha\theta_2' + \theta_2'') \cos \theta_2\},$$

$$G_{44} = \alpha q \sin \theta_4 + \theta_4' \cos \theta_4 - b\{(\alpha^2 q^2 - \theta_4'^2) \sin \theta_4 + (2\alpha q\theta_4' + \theta_4'') \cos \theta_4\}.$$

The requirement of non-vanishing a_i (non-trivial solution) in (23) and (24) leads to the following dispersion relation

$$D_R = \begin{vmatrix} e^{-\alpha} \cos \theta_1 & e^{-\alpha q} \cos \theta_3 & e^{\alpha} \cos \theta_1 & e^{\alpha q} \cos \theta_3 \\ e^{\alpha} \cos \theta_2 & e^{\alpha q} \cos \theta_4 & e^{-\alpha} \cos \theta_2 & e^{-\alpha q} \cos \theta_4 \\ K_{31}e^{-\alpha} & K_{32}e^{-\alpha q} & K_{33}e^{\alpha} & K_{34}e^{\alpha q} \\ K_{41}e^{\alpha} & K_{42}e^{\alpha q} & K_{43}e^{-\alpha} & K_{44}e^{-\alpha q} \end{vmatrix} = 0 \tag{25}$$

and

$$D_I = \begin{vmatrix} -e^{-\alpha} \sin \theta_1 & -e^{-\alpha q} \sin \theta_3 & e^{\alpha} \sin \theta_1 & e^{\alpha q} \sin \theta_3 \\ -e^{\alpha} \sin \theta_2 & -e^{\alpha q} \sin \theta_4 & e^{-\alpha} \sin \theta_2 & e^{-\alpha q} \sin \theta_4 \\ G_{31}e^{-\alpha} & G_{32}e^{-\alpha q} & -G_{33}e^{\alpha} & -G_{34}e^{\alpha q} \\ G_{41}e^{\alpha} & G_{42}e^{\alpha q} & -G_{43}e^{-\alpha} & -G_{44}e^{-\alpha q} \end{vmatrix} = 0, \tag{26}$$

respectively.

A straightforward calculation, presented in Appendix A†, leads to

$$\begin{aligned} D_R = &-e^{2\alpha q + 2\alpha}\{(K_{34} \cos \theta_1 - K_{33} \cos \theta_3)(K_{42} \cos \theta_2 - K_{41} \cos \theta_4)\} \\ &-e^{2\alpha q - 2\alpha}\{(K_{31} \cos \theta_3 - K_{34} \cos \theta_1)(K_{42} \cos \theta_2 - K_{43} \cos \theta_4)\} \\ &-e^{-2\alpha q + 2\alpha}\{(K_{32} \cos \theta_1 - K_{33} \cos \theta_3)(K_{41} \cos \theta_4 - K_{44} \cos \theta_2)\} \\ &-e^{-2\alpha q - 2\alpha}\{(K_{32} \cos \theta_1 - K_{31} \cos \theta_3)(K_{44} \cos \theta_2 - K_{43} \cos \theta_4)\} \\ &-\{(K_{32} - K_{34})(K_{43} - K_{41}) \cos \theta_2 \cos \theta_3 - (K_{33} - K_{31})(K_{44} - K_{42}) \cos \theta_1 \cos \theta_4\}, \end{aligned}$$

and

$$\begin{aligned} D_I = &-e^{2\alpha q + 2\alpha}\{(-G_{34} \sin \theta_1 + G_{33} \sin \theta_3)(-G_{42} \sin \theta_2 + G_{41} \sin \theta_4)\} \\ &-e^{2\alpha q - 2\alpha}\{(-G_{31} \sin \theta_3 + G_{34} \sin \theta_1)(-G_{42} \sin \theta_2 + G_{43} \sin \theta_4)\} \\ &-e^{-2\alpha q + 2\alpha}\{(-G_{32} \sin \theta_1 + G_{33} \sin \theta_3)(-G_{41} \sin \theta_4 + G_{44} \sin \theta_2)\} \\ &-e^{-2\alpha q - 2\alpha}\{(-G_{32} \sin \theta_1 + G_{31} \sin \theta_3)(-G_{44} \sin \theta_2 + G_{43} \sin \theta_4)\} \\ &-\{(-G_{32} + G_{34})(-G_{43} + G_{41}) \sin \theta_2 \sin \theta_3 \\ &\quad - (-G_{33} + G_{31})(-G_{44} + G_{42}) \sin \theta_1 \sin \theta_4\}. \end{aligned}$$

For convenience, we rewrite the expressions for D_R and D_I as

$$\begin{aligned} D_R = -\alpha^2 q^2 e^{2\alpha q + 2\alpha} \Big\{ &\frac{1}{\alpha^2 q^2}(K_{34} \cos \theta_1 - K_{33} \cos \theta_3)(K_{42} \cos \theta_2 - K_{41} \cos \theta_4) \\ &+ \frac{1}{\alpha^2 q^2}e^{-4\alpha}(K_{31} \cos \theta_3 - K_{34} \cos \theta_1)(K_{42} \cos \theta_2 - K_{43} \cos \theta_4) \\ &+ \frac{1}{\alpha^2 q^2}e^{-4\alpha q}(K_{32} \cos \theta_1 - K_{33} \cos \theta_3)(K_{41} \cos \theta_4 - K_{44} \cos \theta_2) \\ &+ \frac{1}{\alpha^2 q^2}e^{-4\alpha q - 4\alpha}(K_{32} \cos \theta_1 - K_{31} \cos \theta_3)(K_{44} \cos \theta_2 - K_{43} \cos \theta_4) \end{aligned}$$

$$+ \frac{1}{\alpha^2 q^2} e^{-2\alpha q - 2\alpha} [(K_{32} - K_{34})(K_{43} - K_{41}) \cos \theta_2 \cos \theta_3$$

$$- (K_{33} - K_{31})(K_{44} - K_{42}) \cos \theta_1 \cos \theta_4] \Bigg\} \tag{27}$$

$$D_I = -\alpha^2 q^2 e^{2\alpha q + 2\alpha} \Bigg\{ \frac{1}{\alpha^2 q^2} (G_{34} \sin \theta_1 - G_{33} \sin \theta_3)(-G_{42} \sin \theta_2 + G_{41} \sin \theta_4)$$

$$+ \frac{1}{\alpha^2 q^2} e^{-4\alpha} (-G_{31} \sin \theta_3 - G_{34} \sin \theta_1)(-G_{42} \sin \theta_2 - G_{43} \sin \theta_4)$$

$$+ \frac{1}{\alpha^2 q^2} e^{-4\alpha q} (-G_{32} \sin \theta_1 - G_{33} \sin \theta_3)(-G_{41} \sin \theta_4 - G_{44} \sin \theta_2)$$

$$+ \frac{1}{\alpha^2 q^2} e^{-4\alpha q - 4\alpha} (-G_{32} \sin \theta_1 + G_{31} \sin \theta_3)(G_{44} \sin \theta_2 - G_{43} \sin \theta_4)$$

$$+ \frac{1}{\alpha^2 q^2} e^{-2\alpha q - 2\alpha} [(-G_{32} - G_{34})(G_{43} + G_{41}) \sin \theta_2 \sin \theta_3$$

$$- (G_{33} + G_{31})(G_{44} + G_{42}) \sin \theta_1 \sin \theta_4] \Bigg\}, \tag{28}$$

which, in the limit $\alpha \to +\infty$, $q > 0$, $q \neq 1$, and under the condition (10), reduces to

$$D_R \to \alpha^2 q^2 b e^{2\alpha q + 2\alpha} \left(1 - \frac{1}{q^2} \right)^2 \cos^2 \theta_1 \cos^2 \theta_3, \tag{29}$$

$$D_I \to \alpha^2 q^2 b e^{2\alpha q + 2\alpha} \left(1 - \frac{1}{q^2} \right)^2 \sin^2 \theta_1 \sin^2 \theta_3. \tag{30}$$

2.3.3. Results

The conditions for D_R and D_I, defined by (27) and (28), respectively, to vanish can be expressed by either $\cos \theta_1 = 0$ and $\sin \theta_3 = 0$ or $\sin \theta_1 = 0$ and $\cos \theta_3 = 0$.

Using the function (14), we can obtain the leading approximation of αc_i and c_r

$$\begin{aligned} \alpha(c_i)_0 &= \frac{\alpha^2 (q^2 - 1)}{Re}, \\ (c_r)_0 &= \frac{c_1}{Re}. \end{aligned} \tag{31}$$

From the expression (31), we have that $q \to 1 + \delta$ where δ is a positive infinitesimal for $\alpha \to +\infty$ if $\alpha(c_i)_0 > 0$. Hence, the asymptotic solutions of (29) and (30) for $\alpha \to +\infty$ and $\alpha b \gg 1$ can be rewritten as either

$$c_0 = -\frac{1}{n\pi + \pi/2} \frac{Re}{\alpha^2 (1 + 2b)}, \quad n = 0, \pm 1, \pm 2, \dots,$$

or

$$\left. \begin{aligned} \alpha(c_i)_0 &= -\frac{1}{n\pi + \pi/2} \frac{1}{1 + 2b}, \quad n = 0, \pm 1, \pm 2, \dots, \\ (c_r)_0 &= \frac{Re}{2m\pi q} + \frac{\frac{2}{3} + 2b}{1 + 2b}, \quad m = \pm 1, \pm 2, \dots, \end{aligned} \right\} \tag{32}$$

or

$$\left.\begin{aligned}
\alpha(c_i)_0 &= -\frac{1}{n\pi}\frac{1}{1+2b}, \quad n = \pm 1, \pm 2, \dots, \\
(c_r)_0 &= \frac{Re}{2(m\pi + \pi/2)q} + \frac{\frac{2}{3}+2b}{1+2b}, \quad m = 0, \pm 1, \pm 2, \dots.
\end{aligned}\right\} \tag{33}$$

From the expressions (32)–(33) and the inequality $b \neq 0$, there exist modes ($n < 0$) such that the growth rate $\alpha(c_i)_0$ satisfies

$$\alpha(c_i)_0 > 0.$$

This means that the problem is unstable for short waves.

2.4. *Stability for long waves*

2.4.1. *The long-wave asymptotic expansion for the Orr–Sommerfeld equation*

In analysing the stability in channels with small Reynolds number, Pekeris (1936, 1948) and Pekeris & Shkoller (1967) expanded the Orr–Sommerfeld equation in terms of a small parameter $\varepsilon = i\alpha Re$. Here, it is a long-wave assumption (very small wavenumber α and small Reynolds number which is generally of the order of $1 \sim 10$ for microchannel flows) that makes the parameter ε small.

Now expand ϕ and $i\alpha Re\, c$ as follows:

$$\phi = \sum \varepsilon^m \phi_m, \tag{34}$$

$$i\alpha Re\, c = \sum \varepsilon^m c_m. \tag{35}$$

Expanding the Orr–Sommerfeld equation (6) leads to

$$\begin{aligned}
&\left(\phi_0^{(4)} + \varepsilon\phi_1^{(4)} + \cdots\right) - 2\alpha^2\left(\phi_0^{(2)} + \varepsilon\phi_1^{(2)} + \cdots\right) + \alpha^4(\phi_0 + \varepsilon\phi_1 + \cdots) \\
&= \varepsilon U\left[\left(\phi_0^{(2)} + \varepsilon\phi_1^{(2)} + \cdots\right) - \alpha^2(\phi_0 + \varepsilon\phi_1 + \cdots)\right] - \varepsilon U^{(2)}(\phi_0 + \varepsilon\phi_1 + \cdots) \\
&\quad - (c_0 + \varepsilon c_1 + \cdots)\left[\left(\phi_0^{(2)} + \varepsilon\phi_1^{(2)} + \cdots\right) - \alpha^2(\phi_0 + \varepsilon\phi_1 + \cdots)\right],
\end{aligned} \tag{36}$$

where $\phi_i^{(n)}$ denotes the nth-order derivative of ϕ_i with respect to y.

The zeroth-order approximation of (36) is

$$(D^2 - \alpha^2 + c_0)(D^2 - \alpha^2)\phi_0 = 0. \tag{37}$$

The stability result will be obtained by using the zeroth-order approximation (37). This is valid for very small ε.

Let ϕ_{0r} and ϕ_{0i} be the real and imaginary parts of ϕ_0, i.e. $\phi_0 = \phi_{0r} + i\phi_{0i}$, then (37) yields

$$(D^2 - \alpha^2 + c_0)(D^2 - \alpha^2)\phi_{0r} = 0. \tag{38}$$

Using (35) and $\varepsilon = i\alpha Re$, we can write

$$i\alpha Re\, c = c_0 + i\alpha Re c_1 + \cdots.$$

If we decompose $c = c_r + ic_i$ where c_r and c_i are real, then the use of the above relation leads to the zeroth approximation of c_i

$$(c_i)_0 = -\frac{c_0}{\alpha Re}. \tag{39}$$

Obviously, if $c_0 > 0$, then $c_i < 0$ and the slip-flow model is stable; if $c_0 < 0$, then $c_i > 0$ and the slip-flow model is unstable.

For convenience, we set $s = i\alpha q$ with $q \geqslant 0$ and let

$$c_0 = \alpha^2 + s^2 = \alpha^2(1 - q^2). \tag{40}$$

Obviously, the model is unstable if $q > 1$ and stable if $q < 1$.

The corresponding zeroth-order approximation of boundary conditions (7) and (8) can also be rewritten as:

$$\phi_{0r} = 0, \quad y = \pm 1, \tag{41}$$

$$D\phi_{0r} = \mp bD^2\phi_{0r}, \quad y = \pm 1. \tag{42}$$

2.4.2. *Solution of the Orr–Sommerfeld equation*

For $q \neq 1$, the general solution of (38) can be expressed as

$$\phi_{0r} = a_1 e^{-\alpha y} + a_2 e^{-q\alpha y} + a_3 e^{\alpha y} + a_4 e^{q\alpha y}. \tag{43}$$

Inserting (43) into (41)–(42) yields

$$a_1 e^{-\alpha} + a_2 e^{-q\alpha} + a_3 e^{\alpha} + a_4 e^{q\alpha} = 0,$$

$$a_1 e^{\alpha} + a_2 e^{q\alpha} + a_3 e^{-\alpha} + a_4 e^{-q\alpha} = 0,$$

$$a_1(-r + r^2 b_1)e^{-\alpha} + a_2(-qr + q^2 r^2 b_1)e^{-q\alpha} + a_3(r + r^2 b_1)e^{\alpha} + a_4(qr + q^2 r^2 b_1)e^{q\alpha} = 0,$$

$$a_1(-r - r^2 b_1)e^{\alpha} + a_2(-qr - q^2 r^2 b_1)e^{q\alpha} + a_3(r - r^2 b_1)e^{-\alpha} + a_4(qr - q^2 r^2 b_1)e^{-q\alpha} = 0,$$

and the requirement of non-vanishing a_i (non-trivial solution) leads to the following dispersion relation

$$D = 0, \tag{44}$$

with

$$D = \begin{vmatrix} e^{-\alpha} & e^{-q\alpha} & e^{\alpha} & e^{q\alpha} \\ e^{\alpha} & e^{q\alpha} & e^{-\alpha} & e^{-q\alpha} \\ (-\alpha + \alpha^2 b)e^{-\alpha} & (-q\alpha + q^2\alpha^2 b)e^{-q\alpha} & (\alpha + \alpha^2 b)e^{\alpha} & (q\alpha + q^2\alpha^2 b)e^{q\alpha} \\ (-\alpha - \alpha^2 b)e^{\alpha} & (-q\alpha - q^2\alpha^2 b)e^{q\alpha} & (\alpha - \alpha^2 b)e^{-\alpha} & (q\alpha - q^2\alpha^2 b)e^{-q\alpha} \end{vmatrix} \tag{45}$$

or (see Appendix B for the detailed derivation)

$$\begin{aligned} D = {} & -2(\eta_1^2 + \eta_2^2)[\cosh(2q\alpha)\cosh(2\alpha) + \sinh(2q\alpha)\sinh(2\alpha)] \\ & - 4\eta_1\eta_2[\sinh(2q\alpha)\cosh(2\alpha) + \cosh(2q\alpha)\sinh(2\alpha)] \\ & + 2(\eta_1^2 + \eta_3^2)[\cosh(2q\alpha)\cosh(2\alpha) - \sinh(2q\alpha)\sinh(2\alpha)] \\ & + 4\eta_1\eta_3[\sinh(2q\alpha)\cosh(2\alpha) - \cosh(2q\alpha)\sinh(2\alpha)] - 8q\alpha^2, \end{aligned} \tag{46}$$

where

$$\eta_1 = (q^2 - 1)\alpha^2 b,$$

$$\eta_2 = (q - 1)\alpha,$$

$$\eta_3 = (q + 1)\alpha.$$

If the expression (44) admits solutions with $q > 1$, then there is instability. However, for any $b > 0$ and $\alpha > 0$, we can show (see Appendix C) that

$$D(q > 1) \neq 0. \tag{47}$$

For the neutrally stable mode $q = 1$, the solutions of (38) should be expressed as

$$\phi_{0r} = a_{11}e^{-\alpha y} + a_{21}ye^{-\alpha y} + a_{31}e^{\alpha y} + a_{41}ye^{\alpha y}. \tag{48}$$

Inserting (48) into the boundary conditions (41)–(42) and the requirement of non-vanishing a_{i1} (non-trivial solution) yields

$$D(q = 1) = (1 + 2\alpha b)^2 e^{4\alpha} + (1 - 2\alpha b)^2 e^{-4\alpha} - 8\alpha^2(1 + 2b + \alpha b + b) - 2. \tag{49}$$
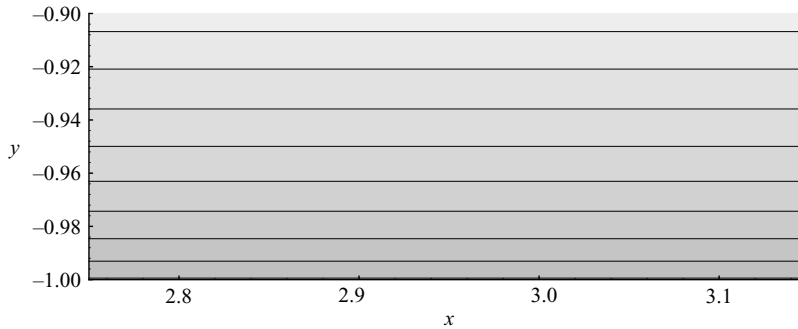
FIGURE 2. Contours for the x-component of the velocity near the lower solid wall for $Kn = 0.0964$ and at instant $t = 0.0002$.

For any $b > 0$ and $\alpha > 0$, we can still show that (see Appendix D)

$$D(q = 1) \neq 0. \qquad (50)$$

By (47) and (50), there is no solution with $q \geqslant 1$, which means that there is no long-wave instability.

3. Numerical simulation of flows in a microchannel

3.1. *Compressible slip-flow model and numerical methods*

We wish to compute numerically the flow in a microchannel as shown in figure 1. We use the compressible Navier–Stokes equations for numerical computation. The slip wall condition is still given by (3). The velocity vector of the basic flow is given by $(U^*, 0, 0)$ where $U^* = U^*(y^*)$. We will use the analytical velocity distribution function as initial condition (the use of other types of initial condition does not affect the results once the flow is established). Arkilic *et al.* (1997) gives details of the velocity distribution functions in a microchannel.

For the numerical method, we have used the robust Godunov scheme (Godunov 1959), extended to second-order accuracy by using the standard MUSCL treatment (Van Leer 1976; Toro 1999), for the inviscid part and a second-order central difference scheme for the viscous part. We will also compute a flow by using the first-order scheme, in order to display that the instability is not a pure numerical one. A Strang splitting (Strang 1968) is used in order to achieve second-order accuracy in time. Some details are given in Appendix E.

The aspect ratio of the microchannel is chosen to be $2H/L = 1/5$. A grid of 150×350 points (350 points in the streamwise direction and 150 points in the transverse direction) is used. Note that the use of a coarse grid cannot capture the unstable waves.

3.2. *Numerical evidence of short-wave instability*

Now we present the numerical result for $Re = 1.0$, $Ma = 0.065$ and $\sigma_v = 0.8$, using the second-order Godunov scheme. In terms of the Knudsen number, this condition corresponds to $Kn = 0.0964$. The numerical solution (using contours of the horizontal-component of the velocity) close to the lower wall at instant $t = 0.0002$ is displayed in figure 2. Similar effects are observed near the upper wall, so we will simply present numerical results close to the lower wall. For this short time, the flow is smooth and no instability has yet developed. At later times, irregular structures develop near the lower wall (also near the upper wall), as can be seen from figure 3 for
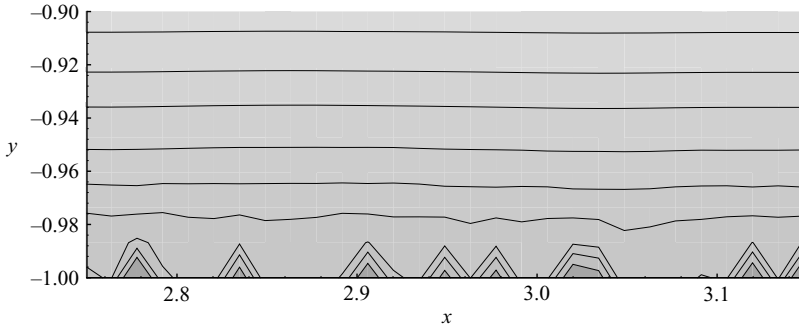
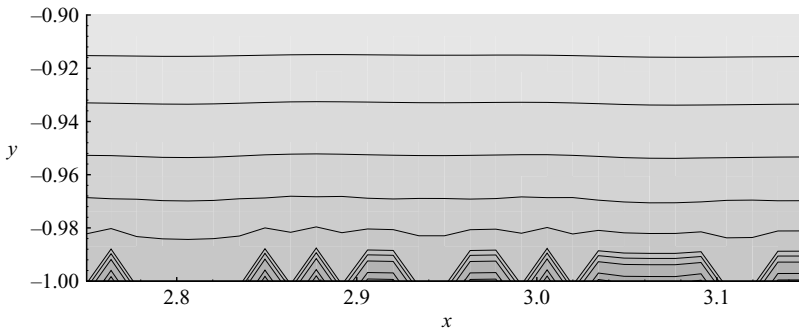FIGURE 3. Contours for the x-component of the velocity for $Kn = 0.0964$ and at instant $t = 0.00125$.

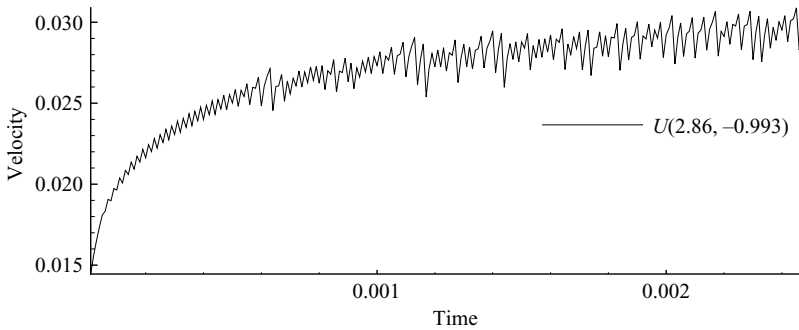FIGURE 4. Contours for the x-component of the velocity for $Kn = 0.0964$ and at instant $t = 0.0025$.

FIGURE 5. Time evolution of the x-component of the velocity at the fixed point $x = 2.86$, $y = -0.993$ for $Kn = 0.0964$. The numerical solution oscillates in time however long we continue the computation.

$t = 00125$ and from figure 4 for $t = 0.0025$. In figure 5, we display the time evolution of the streamwise velocity at the fixed point $x = 2.86$, $y = -0.993$. It is clear that the velocity oscillates in time. The unstable structures clearly reveal that the instability is a short-wave one. The initial increase (or decrease in other conditions) of the mean velocity is due to the initial conditions for numerical computation not being exactly the final solutions (we do not know the exact solution, though we know the velocity profile at steady state). As usual, initial conditions affect the initial stage of linear instability development, but after a long time the (linear) instability is independent of
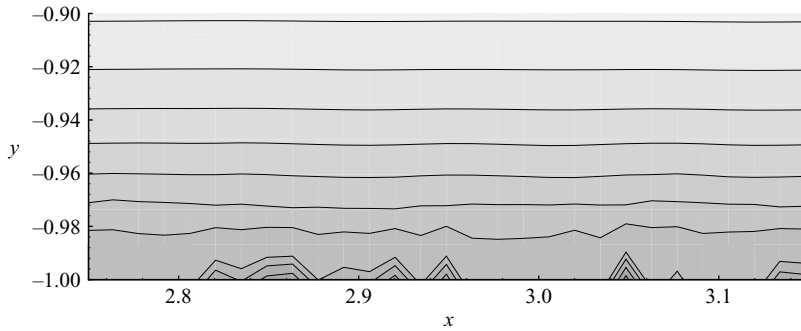
FIGURE 6. Contours for the *x*-component of the velocity ($Re = 1.0$, $Ma = 0.065$) at $t = 0.00125$. Uniform initial data are used.
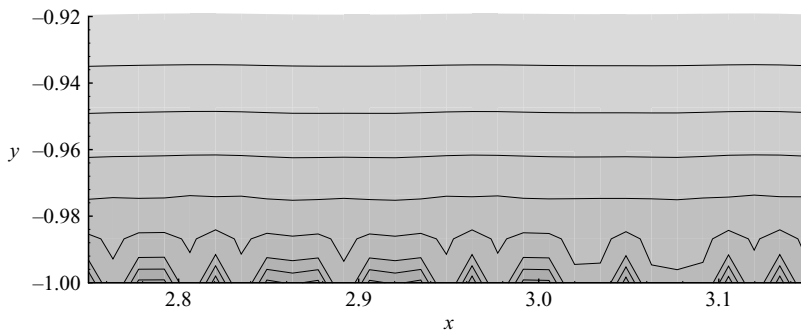

FIGURE 7. Contours for the *x*-component of the velocity at $t = 0.0025$ for $Kn = 0.0964$. This is computed by using the first-order scheme.

the initial condition. In the present case, however, the instability is maintained for as long as we continue the computation. We have also tested different initial data, for instance, the case of a uniform flow. We still observe unstable structures close to the wall (figure 6).

3.3. *Dependence of the instability on numerical accuracy and boundary condition*

We have used a second-order scheme in the previous computation. In order to show that the observed instability is not due to the MUSCL treatment, we display in figure 7 the numerical result at $t = 0.0025$ obtained by the first-order Godunov scheme while keeping the same other conditions as in §3.2. We still observe short-wave instability close to the wall. Hence, the observed instability is not due to numerical treatment.

In fact, the observed instability is due to wall slip (as revealed theoretically). In order to show that wall slip is the origin for the instability, we have performed a computation by using the same condition as in §3.2 while replacing the slip wall condition by the no-slip wall condition (the velocity vanishes on the wall). The numerical result is displayed in figure 8 for the contours of velocity at $t = 0.1$ (a long time after the start of the computation, before this time the computed flow is also stable) and figure 9 for the time evolution at a fixed point. The computed flow is now stable.

We have also computed a flow for $Re = 6.0$, $Ma = 0.3$, and $\sigma_v = 0.8$. This corresponds to $Kn = 0.07415$. If the no-slip wall condition is used, the flow is stable, as shown in figure 10, while the computed flow becomes unstable when the slip boundary condition is used, as displayed in figure 11.
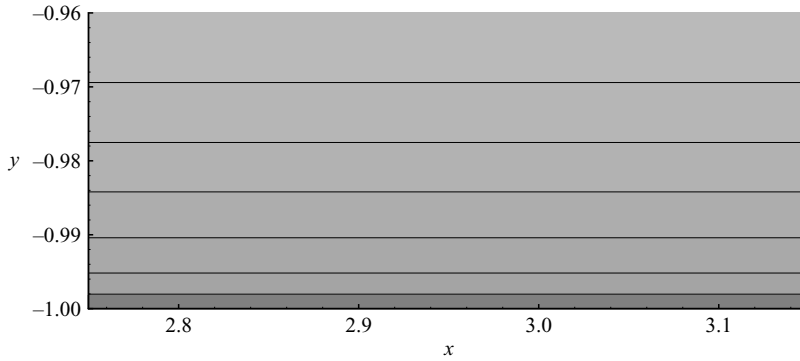
FIGURE 8. Contours for the x-component of the velocity for $K_n = 0.0964$ and at instant $t = 0.1$. The no-slip wall condition is used and the computed flow is always stable.
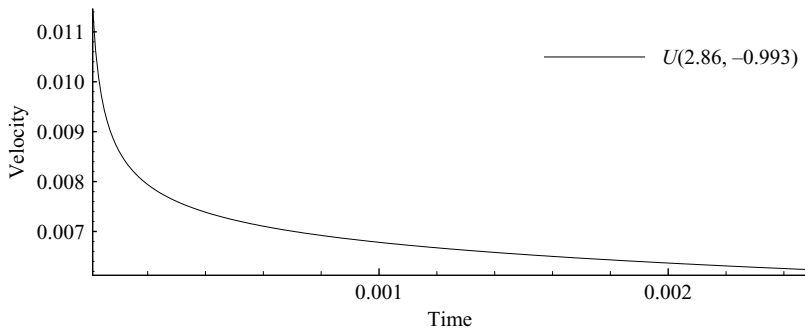

FIGURE 9. Time evolution of the x-component of the velocity for $Kn = 0.0964$ and at the fixed point $x = 2.86$, $y = -0.993$, obtained for the no-slip wall condition. No instability is observed.
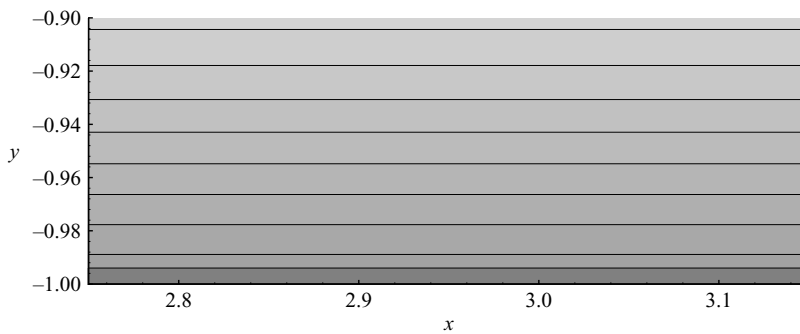

FIGURE 10. Contours for the x-component of the velocity at $t = 0.012$, obtained with the no-slip wall condition: $Re = 6.0$, $Ma = 0.3$ ($Kn = 0.07415$).

3.4. Influence of the Knudsen number

We have computed flows for $Ma = 0.051$ and $Ma = 0.06$ while keeping $\sigma_v = 0.8$ and $Re = 1.0$.

The case $Ma = 0.051$ corresponds to $Kn = 0.0756$. The numerical result for $t = 0.1$ is displayed in figure 12. The computed flow is always stable.

The numerical result is displayed in figure 13 for $Ma = 0.06$, which corresponds to $Kn = 0.089$. The computed flow becomes unstable.
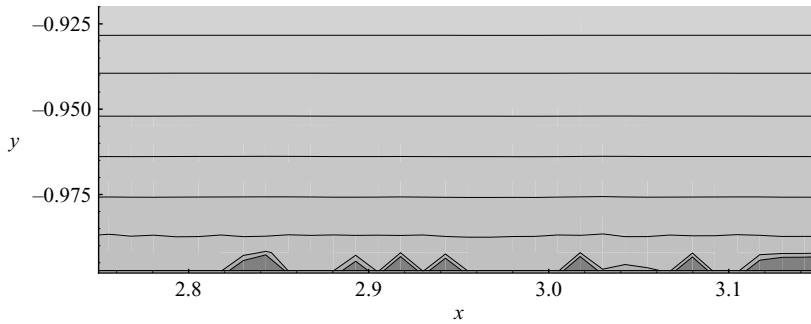
FIGURE 11. Contours for the x-component of the velocity at $t = 0.012$, obtained with the slip wall condition: $Re = 6.0$, $Ma = 0.3$ ($Kn = 0.07415$).
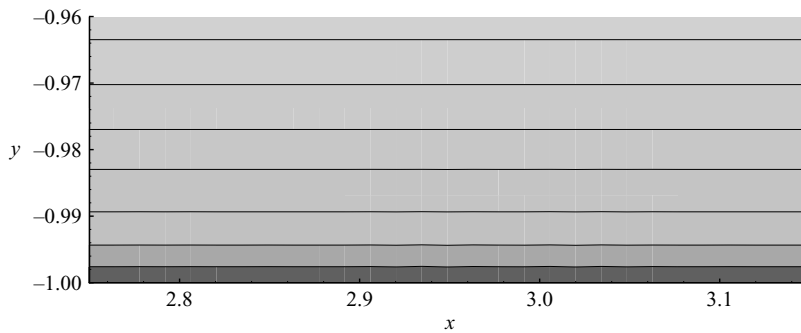

FIGURE 12. Contours for the x-component of the velocity at $Kn = 0.00125$. The flow condition is $Re = 1.0$, $Ma = 0.051$.
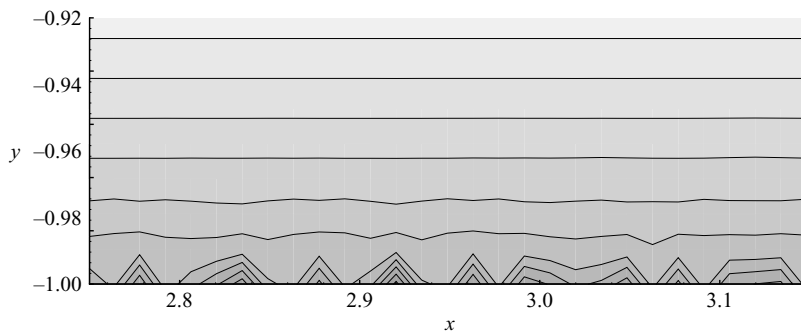

FIGURE 13. Contours for the x-component of the velocity at $t = 0.00125$. The flow condition is $Re = 1.0$, $Ma = 0.06$.

Other computations, not displayed here, show that the computed flow is stable for Ma smaller than 0.051 (or Knudsen number smaller than 0.0756) and unstable for Ma larger than 0.06 (or Knudsen number larger than 0.089).

Now we vary the Reynolds number from $Re = 0.09$ to $Re = 1.16$ while keeping $\sigma_v = 0.8$ and $Ma = 0.065$. In figure 14, we display numerical result for $Re = 1.16$ (which corresponds to $Kn = 0.083$). The computed flow is stable. In figure 15, we display the results for $Re = 0.09$ (which corresponds to $Kn = 0.107$). The computed flow is unstable. Other computations, not displayed here, show that the computed
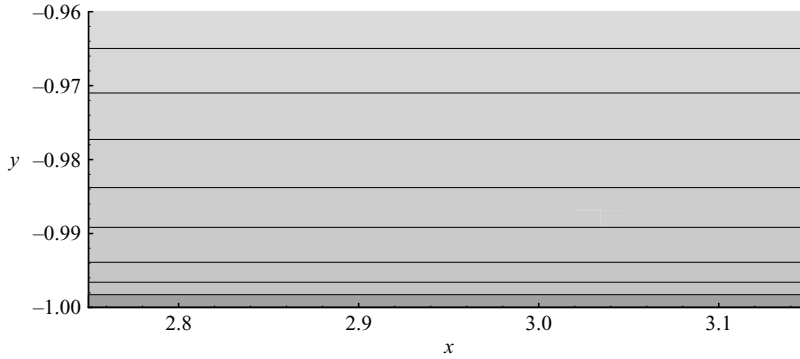
FIGURE 14. Contours for the x-component of the velocity at $t = 0.00125$. The flow condition is $Re = 1.16$, $Ma = 0.065$.
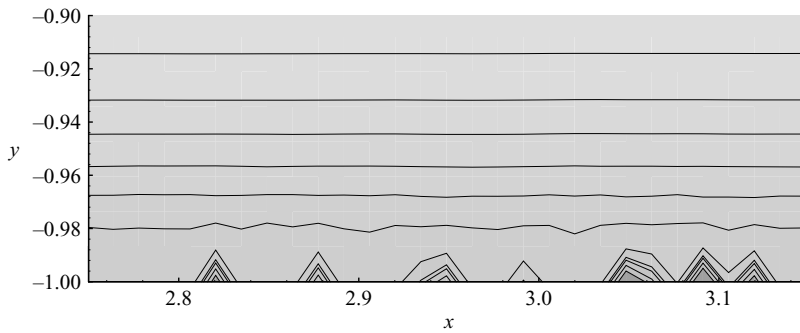

FIGURE 15. Contours for the x-component of the velocity at $t = 0.00125$. The flow condition is $Re = 0.09$, $Ma = 0.065$.

flow is stable for Re larger than 1.16 (or Knudsen number smaller than 0.083) and unstable for Re lower than 0.09 (or Knudsen number larger than 0.107).

Hence, the computed flow is stable for small Knudsen number, while it becomes unstable for large Knudsen number.

4. Concluding remarks and discussion

We have performed a stability analysis using the slip-flow model for flows in a microchannel.

For theoretical analysis, we have simply used the slipflow model for an incompressible and parallel flow. The conclusion is that there is short-wave instability and the model is stable for long waves.

For numerical study we have used the compressible slip-flow model. The numerical results display short-wave instability, as predicted by the incompressible slip-flow model. In our numerical experiments, we have carefully checked that the instability is due to wall slip, and not to numerical instability. When the wall slip is removed, the flow becomes stable in the slip-flow regime.

Hence, either the slip-flow model is unstable, or the problem of microchannel flow is physically unstable in the slip-flow regime.

Similarly to the physical instability, pure model instability is also important. An important example of this type is the so-called Bobylev instability (1982). We know

that flows with moderate rarefaction effect can be described by the Burnett equations. In 1982, Bobylev studied the linear stability of the Burnett equations for Maxwellian molecules and discovered that beyond a certain critical reduced wavenumber there exist normal modes that grow exponentially, concluding that the Burnett equations are linearly unstable. Since then some efforts have been made to construct modified Burnett equations to maintain stability (Zhong, MacCormack & Chapman 1991). Uribe, Velasco & Garcia-Colin (2000) extended the analysis of Bobylev to any interatomic potential and interpreted the instability results in terms of the Knudsen number. They found that there exists a bound for the Knudsen number above which the Burnett equations are unstable. If the present instability (for the slip-flow model) is purely a model instability, caution should be exercised in numerical computations using the slip-flow model. Our experiences shows that unstable waves appear only when the grid is fine enough. If the assumption of pure model instability were true, then further effort would be required to build a stable slip-flow model, similar to the past efforts to modify the Burnett equations.

Though it is not the object of this paper to obtain the critical Knudsen number for instability, our numerical experiments show that the computed flow becomes unstable only when the Knudsen number or slip length b is large enough. It would be important to find the critical Knudsen number for instability. In our short-wave instability analysis, the expansion has been made by requiring b to satisfy (10). Hence, the theoretical analysis holds only when b is not very small. This excludes the possibility of obtaining a critical value for the Knudsen number above which the problem is unstable. The conclusion of the current paper is that when the wavenumber α and the combination αb is large enough, the problem is unstable. Removing the constraint (10) means that lower-order terms must be kept in the analysis so that the asymptotic solutions for the determinants would be much more complex than those given by (29) and (30).

REFERENCES

ARKILIC, E. B., SCHMIDT, M. A. & BREUER, K. S. 1997 Gaseous slip flow in long microchannels. *J. Microelectromech. Systems* **6**, 167–177.

BECHERT, D. W., BRUSE, M., HAGE, W. & MEYER, R. 2000 Fluid mechanics of biological surfaces and their technological applications. *Naturwissenschaften* **87**, 157–171.

BETCHOV, R. & CRIMINALE, W. O. 1967 *Stability of Parallel Flows*. Academic.

BIRD, G. A. 1994 *Molecular Gas Dynamics and the Direct Simulation of Gas flows*. Oxford Science.

BOBYLEV, A. V. 1982 The Chapman–Enskog and Grad methods for solving the Boltzmann equation. *Sov. Phys. Dokl.* **27**, 29–31.

CERCIGNANI, C. 2000 *Rarefied Gas Dynamics: from Basic Concepts to Actual Calculations*. Cambridge University Press.

DRAZIN, P. G. & REID, W. H. 1981 *Hydrodynamic Stability*. Cambridge University Press.

GAD-EL-HAK, M. 1999 The fluid mechanics of microdevices. *J. Fluids Engng* **121**, 5–33.

GODUNOV, S. K. 1959 A finite difference method for the computation of disontinuous solutions of the equations of fluid dynamics. *Mat. Sb.* **47**, 357–393.

GROSSMANN, S. 2000 The onset of shear flow turbulence. *Rev. Mod. Phys.* **72**, 603–617.

HEISENBERG, W. 1924 Uber stabilitat und turbulenz von flussigkeitsstromen. *Annln Phys. Lpz.* **74**, 577–627. (Trans. On stability and turbulence of fluid flows', *Tech. Mem. Natl Adv. Commun. Aero.*, Wash. 1291 1951.)

Ho, C. & Tai, Y. 1998 Micro-electro-mechanical systems (MEMS) and fluid flows. *Annu. Rev. Fluid Mech.* **30**, 579–612.

Hoyt, J. W. 1975 Hydrodynamic drag reduction due to fish slimes. In *Swimming and Flying in Nature*, vol. 2. (ed. T. Y. T. Wu, C. J. Brokaw & C. Brennen). Plenum.

Karniadakis, G. E. & Beskok, A. 2002 Micro Flows Fundamental and Simulation. Springer.

Kennard, E. H. 1938 *Kinetic Theory of Gases,* McGraw-Hill.

Lin, C. C. 1955 *Theory of hydrodynamic Stability*. Cambridge University Press.

Morton M. D. 2001 Extrusion instability and wall slip. *Annu. Rev. Fluid Mech.* **31**, 265–288.

Pekeris, C. L. 1936 On the stability problem in hydrodynamics. *Proc. Camb. Phil. Soc.* **32,** 55–66.

Pekeris, C. L. 1948 Stability of the laminar flow through a straight pipe of circular cross section to infinitesimal disturbances which are symmetrical about the axis of the pipe. *Proc. Natl Acad. Sci. Wash.* **34**, 285–295.

Pekeris, C. L. & Shkoller, B. 1967 Stability of plane Poiseuille flow to periodic disturbance of finite amplitude in the vicinity of the neutral curve. *J. Fluid Mech.* **29,** 31–38.

Schmid, P. J. & Henningson, D. S. 2001 *Stability and Transition in Shear Flows*. Springer.

Shivamoggi, B. K. 1986 Stability of parallel gas flows. Ellis Horwood.

Strang, G. 1968 On the construction and comparison of difference schemes. *SIAM J. Numer. Anal.* **5**, 506–517.

Toro, E. E. 1999 *Riemann Solvers and Numerical Methods for Fluid Dynamics, a Practical Introduction*. Springer.

Uribe, F. J., Velasco, R. M. & Garcia-Colin, L. S. 2000 Bobylev instability. *Phys. Rev.* E. **62**, 5835–5838.

Van Leer, B. 1976 MUSCL, A new approach to numerical gas dynamics. In *Computing in Plasma Physics and Astrophysics*, Max-Planck-Institut fur Plasma Physik, Garchung, Germany, April.

Zhong, X., MacCormack, R. W. & Chapman, D. R. 1991 Stabilization of the Burnett equations and application to high altitude hypersonic flows. *AIAA Paper* 91-0770.